RESEARCH ARTICLE

SPE INSPIRING PLASTICS PROFESSIONALS   Polymer COMPOSITES   WILEY

Development of single-polypropylene composites interleaved with MWCNT-doped melt-blown fine fiber mats

Yahya Kara[1] | Kolos Molnár[1,2]

[1]Faculty of Mechanical Engineering, Department of Polymer Engineering, Budapest University of Technology and Economics, Budapest, Hungary

[2]MTA–BME Research Group for Composite Science and Technology, Budapest, Hungary

Correspondence
Kolos Molnár, Faculty of Mechanical Engineering, Department of Polymer Engineering, Budapest University of Technology and Economics, Műegyetem rkp. 3., H-1111 Budapest, Hungary.
Email: molnar@pt.bme.hu

Abstract

In this article, we demonstrate fabricating polypropylene (PP)/multiwalled carbon nanotube (MWCNT) nanocomposite fiber veils and use them as interleaves in single-polymer composites (SPCs) to enhance their thermal and mechanical properties. With this regard, we produced a hierarchical composite structure made of a film, a woven fabric and a fine fiber mat made of the same polymer. The nanocomposite fiber mats were generated by melt-blowing. Results implied that incorporating MWCNT increased the viscosity of the melt blowing grade PP resin. Increasing MWCNT content increased the average fiber diameter and pore size by 2.1-fold and 2.5-fold, respectively. Incorporating MWCNT enhanced the melt-blown (MB) fiber mat's specific strength by 78% and improved the thermal stability. We generated multiscale SPCs by film-stacking, for which we applied a PP film as a matrix, a PP-woven fabric as the primary reinforcement, and the MB fiber mats as interleaves. The SPC's tensile modulus was improved by 37% by the interleaving. Our findings implied that the MWCNT-doped PP fiber mat interleaving provides a robust interfacial adhesion and higher damage tolerance under tensile load. Master curves were constructed from dynamic mechanical analysis frequency sweep tests based on the time–temperature superposition principle. The storage modulus increased by 33%, while the tanδ decreased around 10% with PP/MWCNT fiber mat interleaving. The developed multiscale SPC with MWCNT fiber mat interleaving veils may be easily integrated into engineering composite applications due to its cost-efficiency, fair recycling, straightforward processing, enhanced stiffness, and interfacial adhesion.

KEYWORDS
carbon nanotube, melt blowing, nanocomposite, recycling, single-polymer composite

1 | INTRODUCTION

Polymeric composites with nanoparticle additives have been extensively investigated for their broad application due to their unique properties, including good adhesion to substrates, high mechanical strength, electrical conductivity, thermal stability, and many more.[1–3] Among the other nanoparticles, carbon nanotubes (CNTs) and their implementation got the great attention of both industry and researchers since their discovery in the late 90s.

The performance of synthetic nano/submicron fibers might be enhanced by nanotube inclusion. For example, one might expect that the CNTs embedded within the fibers may boost the modulus and strength of these fibers. However, achieving uniform dispersion of the nanotubes in a polymer matrix is challenging, and poor dispersion can result in deteriorated properties. This hampers the applicability of CNTs and other nanoparticles in actual industrial applications.[4]

Polypropylene (PP) is broadly utilized in many different products, including twines, ropes, and fine fiber mats.[5–7] Melt-blowing is one of the most suitable methods for producing such PP fine fibers in large volumes. During the COVID-19 pandemic, melt-blowing also gained a lot of attention since this is the most popular method for making the nonwoven filtering layer of protective facemasks and respirators.[8–10] Melt-blowing is a single-step process that directly forms microfibers from a molten polymer through pressurized hot air. If the parameters are set wisely, then submicron and even nanofibers can be produced this way.[11] A wide range of additives and fillers can be mixed into the raw polymer to enhance fiber mat properties, similar to other extrusion-based polymer processing techniques.[8] The melt-blown (MB) fibers have several remarkable advantages, including but not limited to small diameter, high aspect ratio, large specific surface area, networked pore structure, unique physicochemical properties, and design flexibility for chemical/physical surface functionalization.[11,12]

Up to date, various types of nanofillers (graphene oxide, CNTs, nanoclay, etc.) have been incorporated within a polymer matrix to improve the mechanical, thermal and electrical characteristics of fine fiber mats and related composite structures.[13,14] The reinforcing effect of the nanomaterials is complex because they also change the crystallization kinetics, the polymer-additive interfaces and the polymer nanostructure. Hegde and Bhat[15] reported that nanoclay-doped PP MB fiber mats showed high air permeability and low mechanical properties. The nanoclay resulted in a high crystal nucleation density which caused this difference. The crystallization rate of nano clay-doped PP fibers was lower than that of the pristine sample. Hence, the fiber mat's mechanical properties significantly dropped in the presence of nano clay additives. Cao et al.[16] fabricated CNT/PP membranes with enhanced dielectric constant, mechanical properties, and hydrophobicity by melt electrospinning. In their study, CNTs (0.01–0.25 wt%) were first mixed with small amounts of paraffin liquid to enhance spinnability and improve CNT dispersion. The fiber diameter was in the range of 5–10 μm for the neat PP/CNT, while the addition of paraffin liquid slightly decreased fiber diameter. They reported that increasing CNT content caused severe defects and worsening of mechanical properties.

The demand to improve the performance of fiber-reinforced composites, for example, delamination resistance, fracture toughness, stiffness, heat resistance, etc., led to the development of nanotube-reinforced thermoplastic interleaving veils. Dydek et al.[17] generated MWCNT (7 wt %)-doped copolyamid (coPA) MB fiber mats. They reported that the coPA/MWCNT MB fiber diameter was around 100 μm. It is worth mentioning that such a large fiber diameter is unfavorable for interleaving composite laminae because the advantage of the large surface-to-volume ratio is lost. They studied the effect of interleaving MWCNT/coPA MB fiber mats on the carbon/epoxy composite's electrical, thermal and mechanical properties. Their results showed that the electrical volume conductivity increased more than 200% with the MWCNT/coPA MB fiber mat interleaving, while composite laminae storage modulus decreased. Lan et al.[18] developed heat-resistant and durable carbon fiber-reinforced polyimide composites interleaved with thermoplastic polyimide (TPPI) fiber mat. They reported that TPPI fiber mat interleaving (tested at 250°C) enhanced the mode I and mode II fracture toughness of composite laminates over 200% compared to the non-interleaved one. Zhao et al.[19] generated glass and carbon fabric-reinforced polybutylene terephthalate (PBT) hybrid composites with electrospun carbon nanofiber interleaving veil. They made the composites through in-situ polymerization of cyclic butylene terephthalate (CBT) oligomer followed by hot pressing. The interlaminar shear strength, flexural strength, flexural modulus, and work of fracture of the hybrid composites were enhanced by 32%, 25%, 19%, and 33%, respectively, compared to the control samples without nanofiber interleaving veil. All these studies prove that the nano- and submicron fiber interleaving and reinforcing enhance polymer composite laminae performance overall. In addition, incorporating nanoparticles showed great potential to advance fine fiber veils' morphological, thermal, and mechanical properties. However, the method of making nanocomposite fine fiber veils is limited to solution-based processing (e.g., electrospinning, solution blowing) yields low productivity. On the other hand, traditional nonwoven processing like spun bonding is also limited, because either the fiber diameter is over 10 μm or the processing requires multiple steps (e.g., spinning, web formation and bonding).

To the best of our knowledge, so far, no research has been published on fabricating CNT-doped PP MB fine fiber mats. There is also limited research on fine fiber mat-interleaved thermoplastic composites. The demand for developing high-performance thermoplastic composite structures with fair recycling opportunities is rapidly emerging. The new composites research and development era requires multidisciplinary methods comprising nanotechnology, material science, and engineering. In this regard, developing methods for fine fiber generating (e.g., melt blowing) and composite manufacturing (e.g., self-reinforced composites) are favorable for future engineering applications. In this paper, we fabricated PP/MWCNT nanocomposite fine fibers via melt blowing and then created self-reinforced hierarchical composites. The morphological, thermal, and mechanical properties of the nanocomposite fibers are detailed. Findings showed that the fiber mat's thermal and mechanical properties improved by the MWCNT addition. We also investigated the effect of the nanocomposite fine fiber mat interleaving on the thermal and mechanical properties of the SPCs. Our results revealed that the MWCNT/PP fine fiber interleaving notably improved the SPC's mechanical performance.

2 | MATERIALS AND METHODS

2.1 | Materials

HL912FB type PP homopolymer (Borealis, Austria) and low modulus isostatic PP (S401 L-MODU iPP [LiPP], Idemitsu, Japan) were blended in a mass ratio of 9:1 for the preparation of fine fiber mats via melt blowing. A plain-woven PP fabric (Tiszatextil Kft., Hungary) with an areal density of 200 g/m^2 (tape count: 5/cm (warp), 4.2/cm (weft)) was used as the composites' primary reinforcement. A commercially available multiwalled carbon nanotube (MWCNT) Nanocyl™ NC7000 (Nanocyl S.A., Belgium) material was used to prepare PP/MWCNT compound for melt blowing. As the matrix of the composites PP film, LiPP with an R1059A random PPcopolymer (MOL Petrolkémia Zrt., Tiszaújváros, Hungary) were blended in a mass ratio of 1:9. The PP resins properties taken from the technical data sheets provided by the manufacturers are given in Table S1.

2.2 | Producing PP blends for melt-blowing

A PP blend was prepared with a counter-rotating twin-screw extruder (Labtech LE 25–30/C, Thailand) with a composition of 10 wt% LiPP and 90 wt% hPP. A PP/CNT nanocomposite masterbatch was produced with the CNT concentration of

5 wt% and with 47.5 wt% LiPP and 47.5 wt% hPP. To provide fairly good MWCNT dispersion and distribution by melt infiltration (e.g., low viscosity), we produced the masterbatch with high LiPP (MFI: 2600 g/10 at 230°C, 2.16 kg) content. After that, we diluted the masterbatch to CNT concentrations of 0.05, 0.1, 0.25, 0.5, and 0.75 wt% with LiPP and hPP in a mass ratio of 1:9. Even though the LiPP and hPP contents were slightly different for the compound and the masterbatch, the difference, in the end, was negligibly small. We used the same twin-screw extruder for all compounding experiments. The related processing parameters for extrusion blending are given in Table 1. We produced continuous filaments through a double-orifice extruder die, and then we used an LZ-120/VS granulator (Labtech, Thailand), generating granules between 1 and 3 mm.

2.3 | Melt blowing setup used and related processing parameters

For making the MB fibers, a custom laboratory unit was built and applied.[11] A custom dual-slot melt blowing die was mounted to a LE8-24C type single-screw laboratory extruder (LabTech, Thailand). The die operates with 40 fiber-forming capillaries, 330 μm diameter each, arranged in a single row. The die and extruder temperatures were set to 250°C. The air temperature and air pressure were set at 285°C and 2 bar, respectively. The extruder screw speed was set at 5 rpm. The die-to-collector distance (DCD) was set to 300 mm. A drum with a diameter of 160 mm was used as the collector. The drum's circumferential velocity was set at 28 m/min. The sample processing time was 5 min.

2.4 | Extrusion flat film production

For PP matrix film, a PP blend made of 10 wt% L-MODU isotactic PP (iPP) and 90 wt% rPP were produced with a counter-rotating twin-screw extruder, and related processing parameters are given in Table S2. Thin films of the PP blend were prepared with an LF-400 type laboratory extruder followed by a small sheet film line (LabTech LCR300, Thailand). The extruder was equipped with a 200 mm wide coat hanger type die, and the slit distance was set at 0.4 mm. The speeds of the lower and upper take-off rolls were 4 and 3.4 rpm, respectively. The flat film extrusion parameters are detailed in Table S3. The thickness of the film produced was 60 ± 5 μm.

2.5 | Single-polymer nanocomposite production

The aim was to determine the effects of PP/MWCNT fiber mat interleaving on the single-PP composite

TABLE 1 Pristine and MWCNT-doped PP blend extrusion parameters

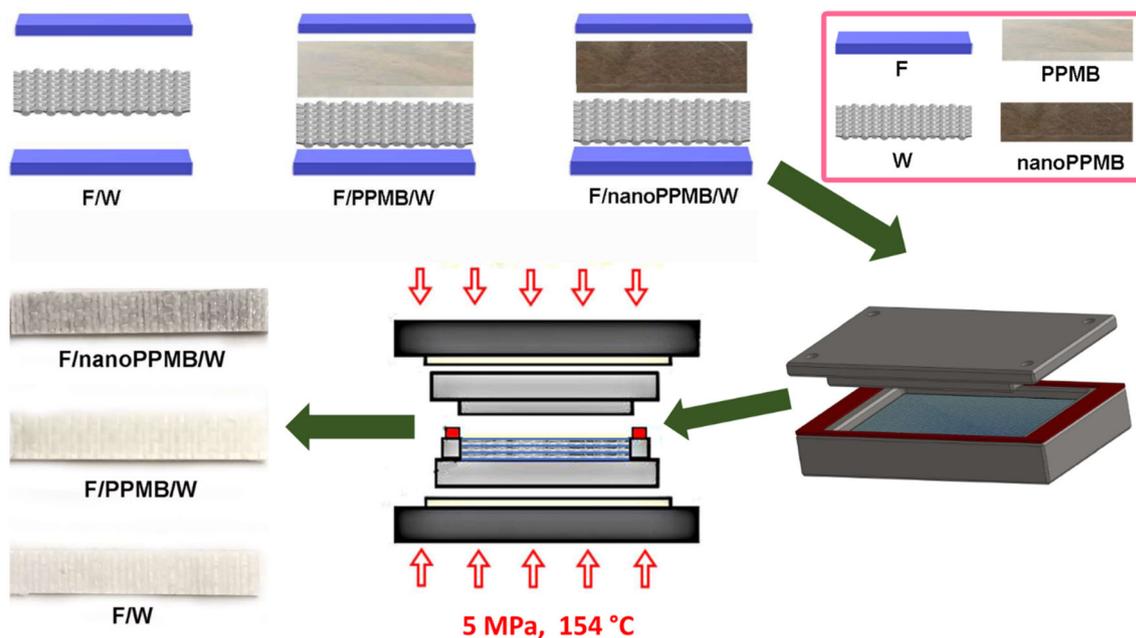| Temperature (°C)											Screw rotation speed (rpm)
Extruder zones											30
1	2	3	4	5	6	7	8	9	10	Die	Feeder speed (rpm)
160	160	160	170	170	170	180	180	190	190	190	7.5

FIGURE 1 Schematic diagram of the SPC production process

performance. For that, we used an MWCNT-doped PP MB fiber mat (nanoPPMB). The blend film (F) was used as a matrix, while woven fabric (W) was the reinforcement for single-PP composite laminates. The reference SPC (F/W) stack consisted of seven layers of PP film (F) and six layers of woven fabric (W), while those SPCs interleaved with PPMB (F/PPMB/W) and nanoPPMB (F/nanoPPMB/W) fiber mats had five layers of fiber mat distributed in between the film and the woven fabric (Figure 1).

The fiber reinforcement and the interleaves were impregnated with the PP matrix film by using a hydraulic hot press, Polystat 300S (Maschienenfabric Fr. Schwabenthan & Co. Kg., Germany). The compression mold consisted of two matching Aluminum halves with a cavity size of 180 mm × 100 mm (length x width). The layered stack was placed into this mold and then put into the hot press set at 154°C (Figure 1). After closing the mold, it was kept for 30 s without pressure to equilibrate the temperature. Then, the compression molding pressure was set at 5 MPa (actual pressure on the specimen) while the holding time was fixed at 120 s. The thickness of the SPC sheets was 2.35 ± 0.1 mm. The PP-woven fiber, PP MB fiber and

matrix film content of the produced composites are given in Table 2.

2.6 | Testing and characterization

The thermal properties of the blends (granules) and the MB fibers were studied by differential scanning calorimetry (DSC), with a Q2000 type (TA Instruments, USA) device. The tests were performed in an inert atmosphere (N$_2$; 50 ml/min purge flow rate) in a temperature range of −50 to 220 °C with a heating and cooling rate (heat ramp) of 10°C/min. The degree of crystallinity (χ) of the fibers was calculated based on Equation (1).:

$$\chi = \frac{\Delta H_m}{\Delta H_m^0} \times 100 \, (\%) \tag{1}$$

where ΔH_m is the experimental heat of fusion obtained by the DSC scans. For the heat of fusion of the 100% crystalline h-PP (ΔH_m^0) 207 J/g was considered[11] in the analysis.

To characterize the PP/MWCNT nanocomposite fiber mat thermal characteristics, TGA was performed using a

TABLE 2 The single-polymer composite samples prepared

Stack description	Woven fabric content (wt%)	Fiber mat veil content (wt%)	Sample code
Film + woven fabric	77 ± 1	–	F/W
Film + woven fabric interleaved with pristine MB fiber mat veil	81 ± 1	5 ± 1	F/PPMB/W
Film + woven fabric interleaved with MWCNT-doped melt-blown fiber mat veil	80 ± 1	4 ± 1	F/nanoPPMB/W

TA Instruments (USA) Q500 type thermogravimetric analyzer between 50°C and 600°C at a heating rate of 10 °C/min under nitrogen purge flow (60 ml/min).

The shear viscosity of the pristine (0 wt%) and CNT-doped (0.1, 0.25 and 0.5 wt%) PP nanocomposites were measured with a capillary rheometer (Instron 13 Ceast SR20). The testing temperature was set to 180°C. We measured the shear viscosity in the 100–7.500 1/s shear rate range, using a capillary with a length and diameter of 20 mm and 1 mm, respectively.

The fibers and composite morphology were observed using scanning electron microscopy (SEM; JEOL 6380 LA, Japan). The surface of the fiber mat and composite samples were finely coated using a JEOL JFC-1200 (Jeol Ltd., Japan) fine coater with gold (Au) to avoid their charging. A total of 100 fibers were measured for each sample to analyze the MB fiber diameter and pore size distributions. We used the ImageJ 1.51 k software for this analysis.

We prepared rectangular samples in 40 mm × 10 mm size. The tensile properties of the fiber mats were tested at room temperature with a Zwick Z005 (Zwick, Germany) type universal tensile tester equipped with a 20 N capacity load cell. The testing routine was performed 7 times for each sample group. The fiber mat length and width were measured using a micrometer (Louis Schopper Leipzig, Germany). Besides, we weighed the PP fiber mat using a Sartorius Quintix 125D-1CEU (Sartorius, Germany) semi-micro scale. We calculated the fiber mat cross-sectional area (A) by using Equation (2).

$$A = \frac{m_{fm}}{l_{fm}\rho_{PP}} \tag{2}$$

where m_{fm} is the fiber mat mass, l_{fm} is the length of the fiber mat, and ρ_{PP} is the bulk density of the PP (0.889 g/cm^3).

The SPCs tensile test was conducted using a Zwick Z250 (Zwick, Germany) test rig with a maximum 250 kN load capability. Samples were cut in 150 mm × 20 mm (length × width). The tensile speed and gauge length were set at 5 mm/min and 90 mm, respectively. A full-field strain measurement was done with a digital image correlation (DIC) method using a Mercury Monet (Sobriety Sro., Kurim, Czech Republic) device. A strain analysis software from Mercury RT-v2.6 was used for local strain measurement. We examined seven samples for each group and analyzed the tensile modulus, the tensile strength, and the strain at break according to the ISO 527-4:2021.[20]

Dynamic mechanical thermal analysis (DMA) of the SPCs was carried out with a DMA Q800 type device (TA Instruments, USA) in three-point bending mode. The frequency, the testing temperature range and the heating rate were 1 Hz, 30–110°C, and 3°C/min, respectively. Samples were cut in 60 × 10 mm (length × width). The small-amplitude frequency-sweep experiments were performed between 1 and 100 Hz (10 points per decade with a logarithmic increment) at different temperatures ranging from 30 to 110°C (10°C increments). The strain amplitude was 20 µm. The results obtained were used to generate master curves using the time–temperature superposition (TTS) principle.[21] The set of curves obtained at various temperatures was shifted horizontally using the Williams–Landel–Ferry (WLF) equation (Equation (3)).

$$\log a_t = \frac{-C_1(T - T_{\text{ref}})}{C_2 + (T - T_{\text{ref}})}, \tag{3}$$

where C_1 (−) and C_2 (K) are constants, a_t is the shit factor, T_{ref} is the reference temperature (K), and T is the arbitrary temperature (K).

3 | RESULTS AND DISCUSSION

3.1 | Analyzing PP/MWCNT blends rheology and thermal properties

We prepared a masterbatch and blends for making fibers via melt blowing. We made a binary PP compound that consisted of commercial grade iPP and low viscosity and low modulus LiPP in a mass ratio of 1:1 to prepare a

masterbatch consisting of 5 wt% MWCNT. Then, we prepared PP/MWCNT nanocomposite blends with the masterbatch for melt blowing by the twin-screw extruder. In general, the high melt viscosity generates higher shear stresses, which helps reduce the MWCNT agglomerates' size. This phenomenon is known as agglomerate rupturing. On the other hand, the recent studies showed that the dispersion of MWCNT agglomerates could also be achieved by eroding the particles from the agglomerate surface.[22,23] Better melt infiltration may lead to erosion of agglomerates, which gives, in turn, efficient nanoparticle dispersion. In this regard, lower polymer melt viscosity may translate into an effective infiltration process (i.e., high molecular flexibility and mobility).[22,23] On the other hand, incorporating nanoparticles and fillers into the polymer matrix increases the polymer viscosity.[24,25] Melt blowing requires low polymer melt viscosity for attenuating polymer jets into thinner fibers. The high melt viscosity yields the formation of larger fibers and defects; hence, the advantage of the process of forming fine fibers is lost. Therefore, the aim for preparing melt blowing nanocomposite blend (MWCNT/iPP/LiPP) was to lower the melt viscosity to allow fair dispersion of MWCNTs within the matrix and still be able to generate fine fibers.[26,27]

We analyzed the pristine and the nanocomposite blends' properties via capillary rheometry and DSC prior to melt blowing. DSC results (Figure 2 and Table S4)

showed that the crystalline melting temperature slightly shifted to higher levels with MWCNT doping, while the crystalline melting enthalpy slightly increased. This increase might be related to the nucleating effect introduced by the MWCNTs, resulting in thicker lamellae and smaller crystal size.[28] Consequently, this can cause a slight increase in the peak crystalline melting temperature. We observed that the onset and peak crystallization temperatures shifted to a higher temperature in the cooling cycle with increasing MWCNT content (Figure 2 A). This also indicates the nucleation effect of MWCNT within the polymer matrix.[29,30] The second heating cycle melting characteristics revealed that MWCNT restricted the molecular mobility and suppressed the crystalline phase transition in the PP matrix. On the other hand, the pristine PP blend showed a double melting endotherm that indicates crystalline phase transition from the stable α phase (monoclinic) to the mesomorphic form. The mesophase can form at cooling rates high enough to prevent the crystallization of the more stable monoclinic α form.[11,31] Results implied that the CNT addition suppressed the crystalline phase transition and resulted in monoclinic α crystalline form.

Melt viscosity is critical in generating MB fibers and also influences fiber characteristics. Findings showed an obvious shear-thinning characteristic for all the PP blends over the investigated shearing range. Melt blowing utilizes high shear rates to draw the polymer melt onto
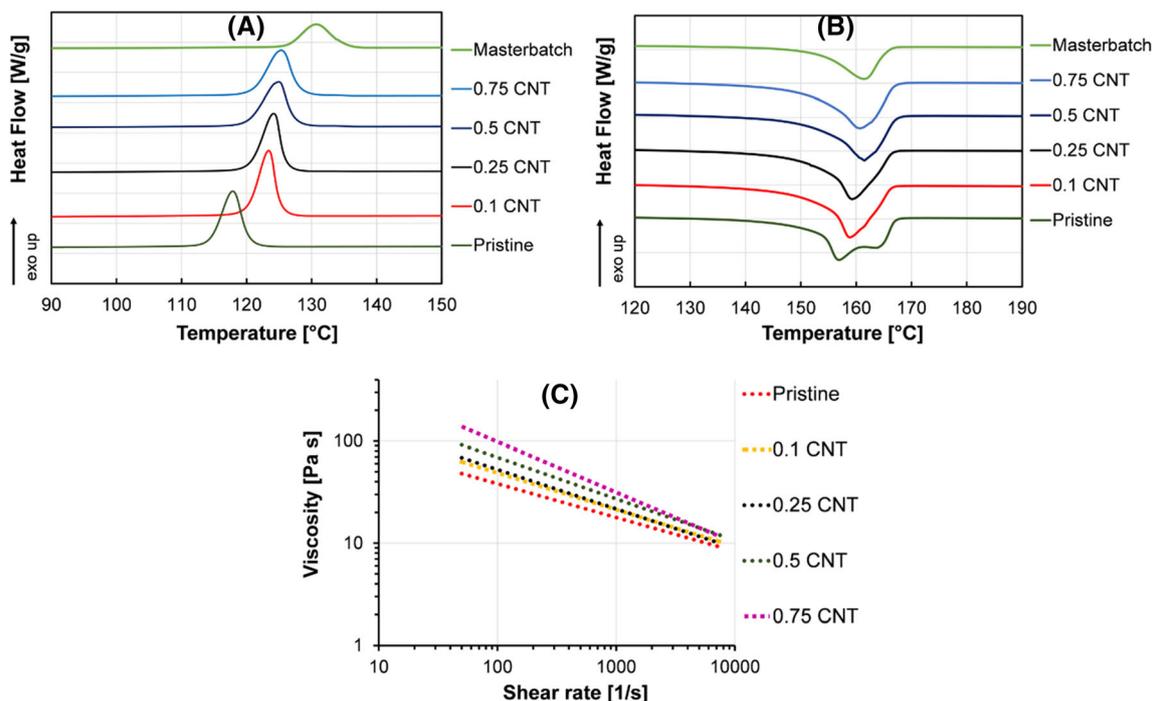

FIGURE 2 DSC thermograms of the pristine and MWCNT-doped blends, (A) cooling, (B) 2nd heating, and (C) variation of nanocomposite PP blend viscosity versus the shear rate at 180°C

fine fibers.[32,33] MWCNT addition significantly increased the shear viscosity, as shown in Figure 2 (c). This phenomenon indicates that the MWCNT doping confined the molecular mobility. Increasing viscosity can be attributed to the dispersion and interaction of the MWCNTs with the polymer matrix. The difference in viscosity becomes lesser with increasing shear rates due to the breakdown and alignment of the MWCNT network.

3.2 | Analysis of nanocomposite MB fiber mat morphology, thermal, and mechanical properties

We generated fiber mats with various MWCNT contents ranging from 0 to 0.75 wt%. The optical and SEM images of the fiber mats are shown in Figure 3. We were able to generate continuous nanocomposite fibers up to 0.5 wt% MWCNT loading. The 0.75 wt% MWCNT-doped PP resulted in melt shots rather than fibers, as shown in Figure 3E and Figure S1. Therefore, 0.75 wt% MWCNT-doped PP fiber mat was not included for further analysis. Attenuating the polymer melt into fine fibers by the pressurized hot air became difficult with high MWCNT content due to increased melt viscosity (Table S5). The higher the viscosity, the higher the fiber diameter (Figure 4A and Figure S2), the pore size (Figure 4B and Figure S3), while the fiber mat surface density decreases (Figure S4).

In melt blowing, increasing viscosity is proportional to the fiber diameter and pore size.[8,34,35] The same hot air drag and drawing force cannot attenuate the polymer melt with different viscosities to the same extent.[8] Therefore, the fiber structure and property are greatly affected by polymer viscosity.[11] Increasing polymer viscosity with the presence of MWCNT makes the shearing and disentanglement of molecules harder. Our results revealed that increasing MWCNT content increased polymer viscosity and reduced drawing rate. Larger fibers yielded larger pores and lower fiber surface density with an increasing MWCNT content. Besides, thinner fibers cool faster, resulting in evenly distributed and high quality (i.e., oriented, enhanced mechanical, thermal properties, etc.) fine fiber mats.[11] Fiber mats with a larger diameter cool at a slower rate; therefore, this phenomenon might also cause defects and irregularities, for example, melt fusion and fiber shots.

DSC tests (Figure 5, Figure S5, Tables S6 and S7) revealed that the PP/MWNT nanocomposite fiber crystallization begins at a temperature higher than that of pristine PP, as shown in Figure 5B. The pristine fiber mat showed a single endotherm during the melting event, as shown in Figure 5A, while the blend had double peaks (Figure 2B). This finding implies that the fiber mat has improved intrinsic orderliness compared to the blend. The peak crystallization temperature shifted to higher levels (up to 7°C) with MWCNT loading compared to the pristine fibers. These results reveal that the MWCNT
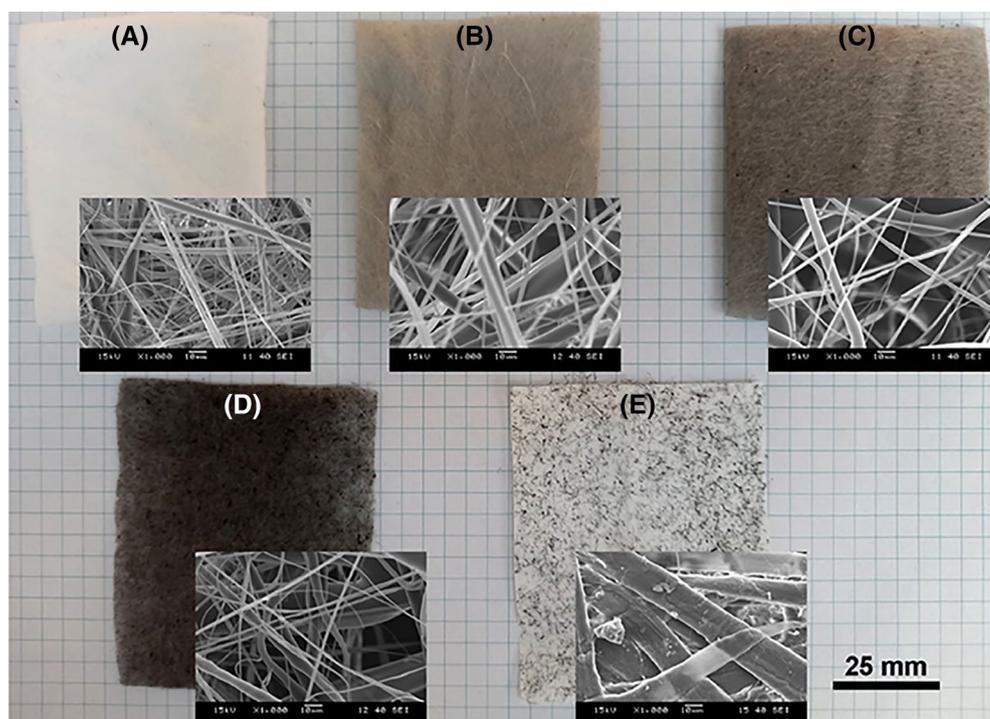

FIGURE 3 Optical and SEM images of MB fiber mats: (A) pristine, (B) 0.1 wt% CNT, (b) 0.25 wt%, (D) 0.5 wt% CNT, and (E) 0.75 wt% CNT
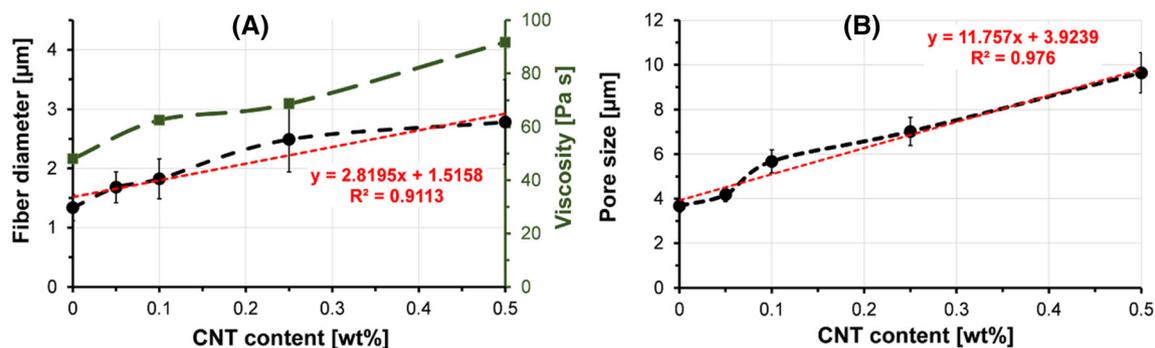
FIGURE 4 Effect of MWCNT content on the (A) fiber diameter, shear viscosity at 50 1/s and (B) pore size
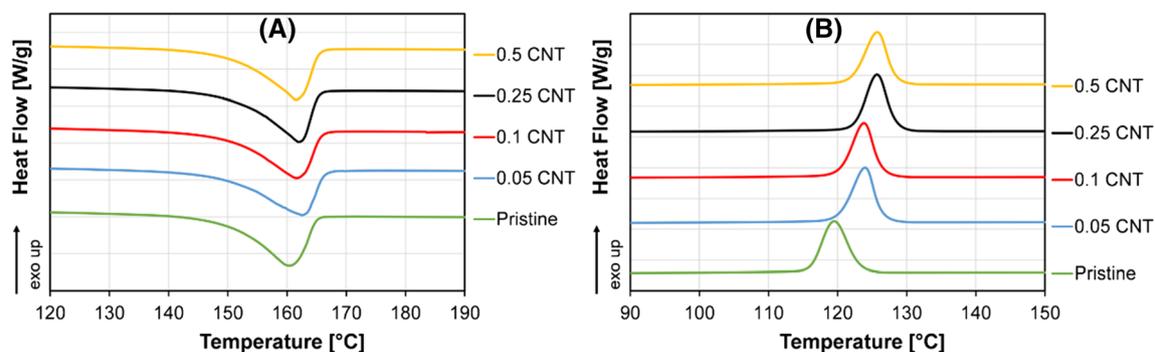

FIGURE 5 DSC thermograms of the fiber mats; (A) 1st heating and (B) cooling

doping resulted in the nucleation and growth of crystals in the PP matrix.[16,22,36] However, no significant change in the crystallization enthalpy was observed since MWCNT content was very low (≤0.5 wt%). This might be sourced by the intrinsically highly oriented molecular fiber structure that maintains the crystallinity.

As the MWCNT loadings increased, the degree of crystallinity decreased negligibly. These may be attributed to increasing the quantity of the molecular entanglements and nucleation of the PP crystallites caused by the MWCNT addition.[37,38] On the other hand, the first heating crystalline melting temperature slightly increased, approx. 1.5–2 °C, increasing MWCNT content compared to the pristine PP fiber mat (Figure 5A). Similar to blends, pristine MB fibers showed a double melting endotherm, indicating crystalline phase transition in the second heating scans (i.e., removal of the thermal history). On the other hand, we found that the crystalline melting temperature of the fibers was shifted by around 1–1.5°C to higher temperatures than at the nanocomposite blends (Table S4 Table S7). The crystalline melting enthalpy of the 0.5 wt% MWCNT-added fiber mat increased by approximately 3% (from ∼40% to ∼43%) compared to the blend (the same 0.5 wt% MWCNT content). However, no significant change is observed in peak crystalline melting temperature and enthalpy.

The rate of crystallization, heat transfer mechanism, cooling rate, and kinetics were different in the presence of the MWCNT. Increasing MWCNT content might be led to faster cooling of the fibers.[15,36,39] A higher cooling rate causes individual fibers to solidify faster compared with pristine fibers, which reduces the extent of interfacial bonding between fibers.[40–42] Therefore, the fiber mat's specific strength significantly dropped with increasing MWCNT content. Besides, decreasing fiber surface density with increasing MWCNT content also worsened the nanocomposite fiber mat's strength. MWCNT loading increased the fiber diameter and pore size. Thicker fibers with high MWCNT content yielded fewer entanglements due to their higher bending stiffness, which dropped the fiber mat strength.[8] With an increasing MWCNT loading, the nanotube-rich areas become bigger, forming clusters/agglomerations. This phenomenon renders decreasing the fiber mat strength due to debonding and stress concentration around the MWCNT agglomerations. In addition, MWCNT agglomerations and fiber shots were observed (Figure 3 and Figure S1), which can also explain the deterioration of the mechanical properties.

TGA results showed that PP degrades in a single step, which begins around 300°C. Beyond 300°C, the degradation was significantly influenced by the MWCNT loading.

The MWCNT loading increased the onset of thermal decomposition values (e.g., at the 5% weight loss) and the nanocomposite gained a maximum onset of 402°C, as shown in Figure 6 and Table S8. The MWCNT doping increased nanocomposite fiber mat's onset thermal degradation temperature between 55°C and 77°C that of pristine one. This improvement in thermal stability might be attributed to the fairly good matrix–nanotube interaction and the thermal conductivity of the nanotubes. Since CNTs have good thermal conductivity, the MWCNT could easily take up the heat applied to the nanocomposite fibers. Besides, MWCNT dispersion in the polymer matrix might induce the spreading of heat uniformly along with the fiber, resulting in enhanced thermal stability.[30,37,43,44]

Nanocomposite fiber mat with 0.05 and 0.1 wt% MWCNT showed significantly higher specific strength compared to the pristine one (Table 3 and Figure S6).
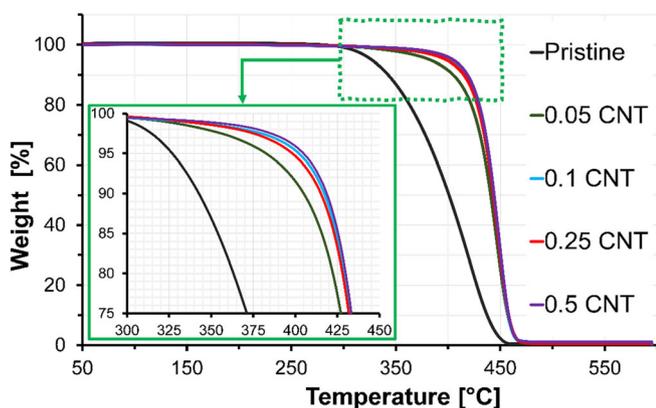

FIGURE 6 TGA curves of the pristine and nanocomposite fiber mats

TABLE 3 Variation of fiber surface density and specific strength versus MWCNT content

MWCNT content (wt%)	Fiber surface density (g/m²)	Specific strength (kN/mg)
Pristine	217.7 ± 27.8	12.5 ± 3.0
0.05	120.6 ± 8.7	15.6 ± 2.0
0.10	114.6 ± 9.0	22.3 ± 1.4
0.25	71.1 ± 7.5	13.8 ± 2.2
0.50	51.7 ± 2.0	8.7 ± 1.0

TABLE 4 DSC 1st heating data of blend film and woven fabric

	1st heating crystalline peak melting temperature (°C)	1st heating melting enthalpy (W/g)	Degree of crystallinity (%)
PP-woven fabric	168.0	117.8	56.9
PP Blend film	146.3	54.5	26.3

When the MWCNT content was 0.1 wt.%, the specific strength significantly improved among the other samples. This finding suggests that the nanoparticle's homogenous dispersion might be limited to 0.1 wt%. After this point, specific strength continuously decreased as MWCNT content increased. The fiber surface density is generally proportional to the fiber mat strength due to the number of fiber entanglements. However, the intrinsic properties also influence the fiber mat performance. Results revealed that adding 0.1 wt%, MWCNT resulted in 78% higher specific strength, while the fiber surface density was 90% lower than that of the pristine one (Table 3, Figure S7). This improvement could be handy for applications where lightweight is essential. On the other hand, thinner fibers resulted in higher strength. This might be related to the shearing of the polymer melt, which in turn gave a more homogenous distribution of nanotubes during the melt blowing. Results revealed that increasing MWCNT doping caused increased viscosity that generated thick and defective fibers, resulting in weaker mechanical properties. We concluded that the 0.1%wt CNT doping resulted in the best morphological, thermal and mechanical properties (Figure S6). Therefore, we chose the 0.1%wt-doped PP MB fiber mat for the composite interleaving study.

3.3 | Analysis of MWCNT/PP MB nanocomposite fiber mat-interleaved single-PP composites

We produced SPCs by interleaving those with MB nanocomposite fiber mat veils. For that, we used 0.1 wt% MWCNT-doped PP MB fiber mat (F/nanoPPMB/W) only since it showed significant improvement in specific tensile strength. It was compared with the pristine PP MB fiber mat-interleaved SPC (F/PPMB/W) and SPC without an interleaving fibrous veil (F/W). The PP-woven fabric and PP blend film's DSC 1st heating scan data are given in Table 4, while DSC thermograms are shown in Figure S8.

3.3.1 | SPC's tensile properties

We investigated the produced SPC's tensile properties using the DIC method. Results showed that the highest
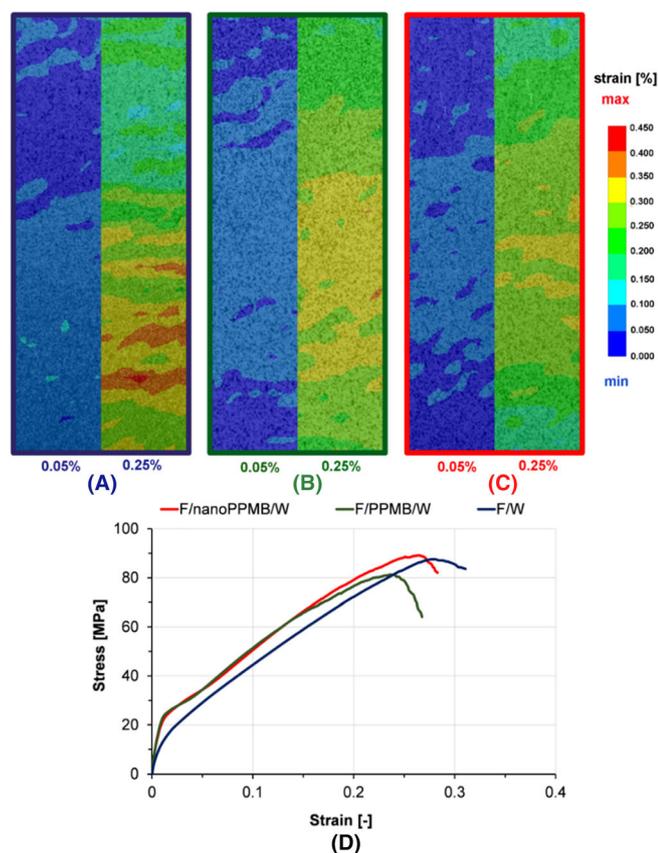
FIGURE 7 Tensile modulus range local strain fields of the SPCs for (a) F/W, (B) F/PPMB/W, (C) F/nanoPPMB/W, and (D) stress–strain curves of all SPCs

TABLE 5 Tensile test data

	Tensile modulus (E_t) (GPa)	Tensile strength (σ_{UTS}) (MPa)
F/W	1.9 ± 0.1	87.5 ± 7.1
F/PPMB/W	2.5 ± 0.2	82.1 ± 6.7
F/nanoPPMB/W	2.6 ± 0.1	89.1 ± 3.2

Tensile modulus (i.e., elastic modulus, Young's modulus) is a key parameter in engineering design and materials development. The DIC strain field analysis showed that F/W SPC had higher strains in the elastic modulus range (0.05%–0.25%). Results showed that the local strains were distributed on the surface for interleaved specimens. On the other hand, non-interleaved laminate (F/W) had a concentrated and highest strain toward the transverse direction. This also implies that the consolidation was better for the interleaved SPCs than for the F/W. The MB fiber mat interleaving restricted the severe failure mechanisms, like tape-debonding (Figure 7 [A–C]). This improvement is attributed to improved laminate stiffness by enhancing interfacial strength. However, the local strains were more distributed (Figure 7C) due to enhanced stiffness and interfacial strength, but the highest strains were still concentrated in the areas of the surface transverse tape. Nevertheless, the recorded highest strains for the interleaved SPCs were lower than for the non-interleaved ones for the tensile modulus range.

The randomly and evenly distributed fine fibers predominantly suppressed the severe fracture in the tensile event. This improvement was also ought to MB fiber's large surface-to-volume ratio. The MB fine fibers bridging (Figure 8D) created lower strains in the interface, increasing load-bearing capacity. The fiber-matrix interfacial interactions determine the polymer composite's structural integrity and overall performance against various loading conditions. Incorporating PP/MWCNT nanocomposite fiber mat veil also caused restriction sites at a molecular level, which prevented the SPC from deforming at high loads. The stiffness improvement by incorporating nanocomposite fiber was more pronounced at higher load levels. Results showed that the non-interleaved laminate had intensive and high local strains propagating through the edges in multiple regions (Figure 8A). The interleaved SPCs exhibited rather distributed the highest strains, owing to enhanced interfacial properties. On the other hand, F/nanoPPMB/W SPC showed a lower strain and a more distributed local strain field than the F/W and F/PPMB/W, as shown in Figure 8A–C. These results indicate that the PP/MWCNT fiber mat interleaving veil enhances the interaction between the reinforcement and polymers, increasing the composite structure's load-carrying capacity.
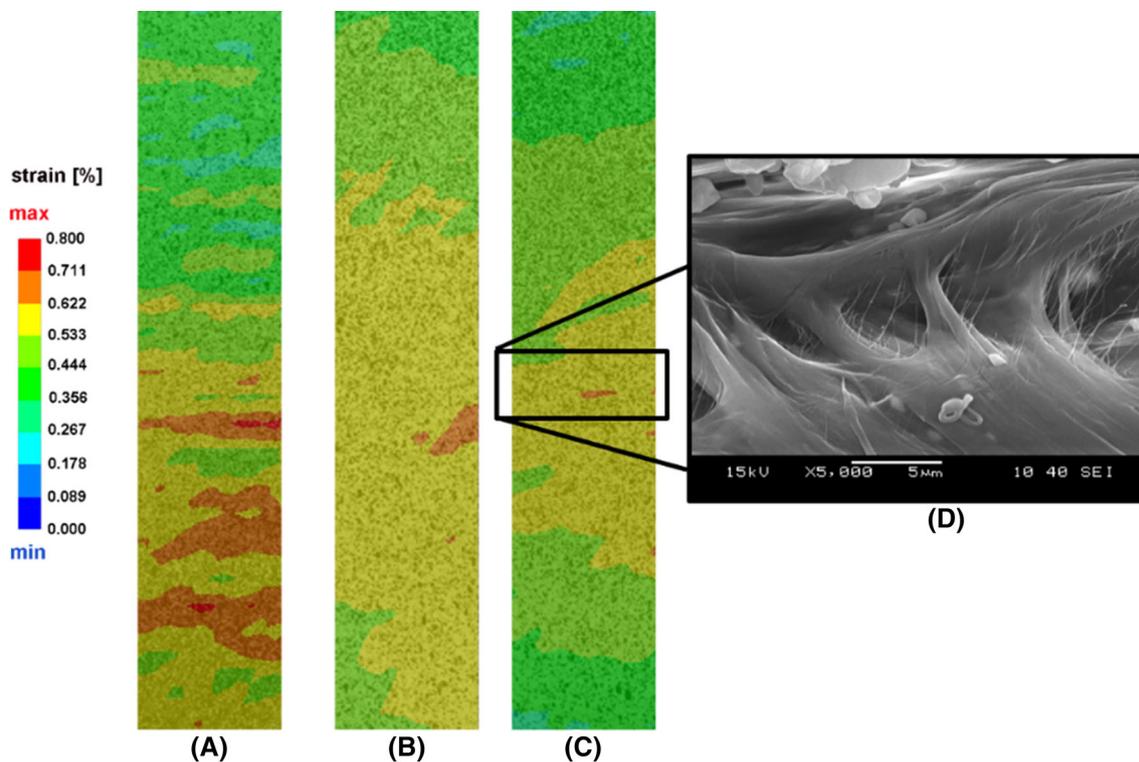
tensile strength and tensile modulus were recorded for the F/nanoPPMB/W SPC. The tensile modulus of the two interleaved composites was similar, while the CNT addition slightly improved the tensile strength (by ∼7%), as shown in Figure 7 and Table 5.

The decrease in tensile strength in the case of F/PPMB/W might be related to the difference between the strength of the fiber mat interleaves and the matrix-reinforcement phases. The interleaved SPCs had a significantly higher load-bearing capacity at the low strain range, where tensile modulus was determined (Figure 7 [A–C]). In addition, F/W SPC's tensile modulus was found slightly higher than F/PPMB/W one. Results implied that interleaved SPCs had lower strain at break, indicating ductile to brittle transition (i.e., stiffened matrix-reinforcement interphase), as shown in Figure 7 (d). Decreased strain at break was accompanied by the noticeable increase in modulus attributed to the improved interfacial adhesion and fine fibers veil's reinforcing effect.[45] We found that the non-interleaved SPC had nearly 24% lower tensile modulus than interleaved SPCs. This finding proves that the nanocomposite fine fiber mat interleaving method established a fairly good interfacial adhesion, resulting in stiffer laminae.

FIGURE 8 DIC contours of SPCs (a) F/W, (B) F/PPMB/W, (C) F/nanoPPMB/W at 0.5% local strain, and (D) SEM image of the F/nanoPPMB/W nanocomposite fiber mat-matrix interface
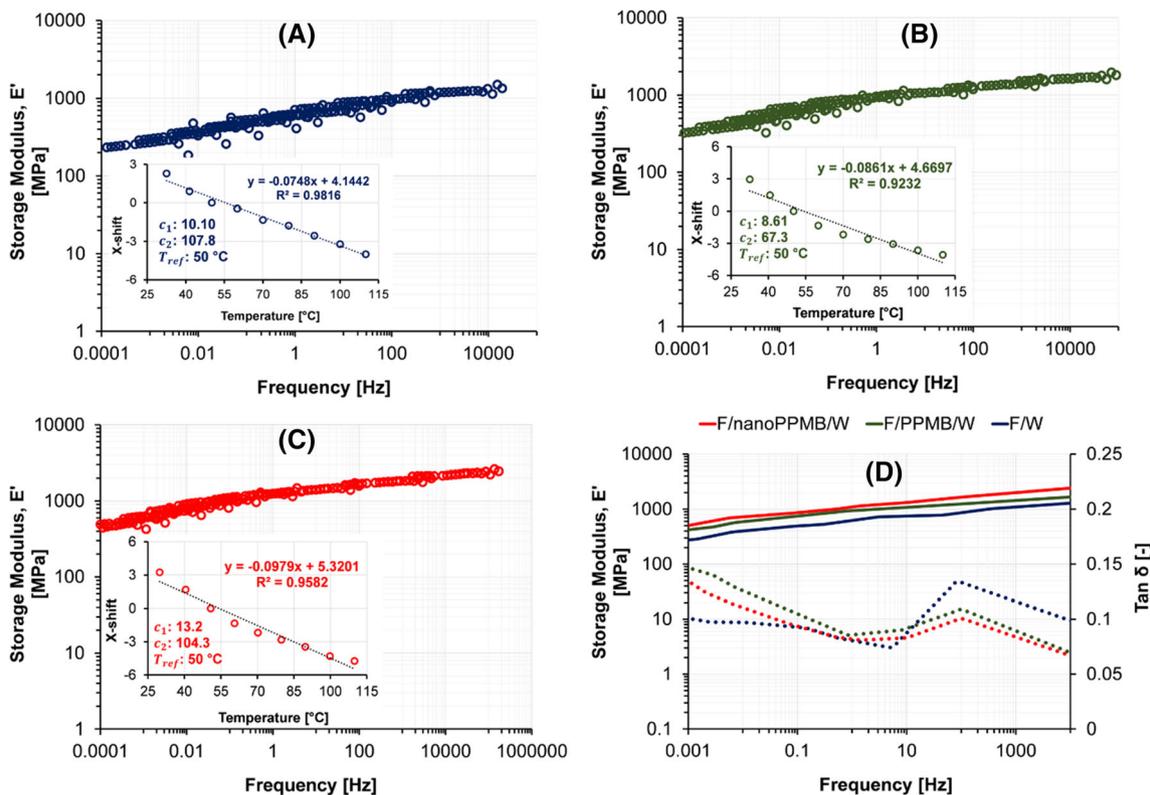

FIGURE 9 DMA curves of SPCs: Storage modulus, E', with respect to frequency data shifts based on the time–temperature superposition (TTS) (a) F/W SPC, (B) F/PPMB/W SPC, (C) F/nanoPPMB/W, and (D) storage modulus and tan δ versus frequency master curves of the SPCs at a reference temperature of 50 °C

3.3.2 | DMA frequency-sweep test results

The SPCs dynamic mechanical performance was examined by frequency sweep tests and the time–temperature superposition (TTS) principle. The DMA frequency sweep curves were shifted to create a master curve at a reference temperature of 50°C by using the WLF equation. The shifted data points and corresponding a_t (x-shift) factors of the composites are shown in Figure 9A–C.

The matrix-reinforcement interface characteristics are directly related to the dissipation and storage of strain energy. In this regard, a poor interface dissipates more energy and might increase the tan δ (i.e., viscous energy) due to the frictional dissipation mechanism.[46] A rigid/elastic behavior was observed in all SPCs as frequency rose (Figure 9). On the other hand, the MB fiber mat-interleaved SPCs (F/PPMB/W and F/nanoPPMB/W) showed lower tanδ compared to that of the non-interleaved one. The relaxation of polymer chain segments was reduced with the MB fiber mat interleaving, while we observed a further decrease with nanocomposite fiber mat-interleaved SPC. F/W, F/PPMB/W and F/nanoPPMBN/W SPCs tanδ were found to be 0.13, 0.11, and 0.10, respectively. Incorporating a nanocomposite fiber mat veil resulted in interconnected structures and restrained the segment mobility of the matrix molecules, resulting in reduced tan δ and improved storage modulus.

The mechanical energy dissipation ability of composite laminae is one of the key factors in designing composite structures for engineering applications.[47] Enhanced storage modulus and reduced tanδ by interleaving imply the dominant elastic character of the SPCs at a higher frequency prevailing over a viscous behavior. F/W, F/PPMB/W, and F/nanoPPMBN/W SPCs storage modulus at peak tanδ were 783, 1246, and 1659 MPa, respectively. In addition, these results are in-line with tensile test findings, which implies enhanced laminate stiffness by the MB fiber interleaving. These results implied that incorporating PP/MWCNT nanocomposite fibers interleaving veils provided a more robust interfacial adhesion, translating to a higher storage modulus and lower tanδ of the SPCs.

4 | CONCLUSION

We studied the structure and morphology, thermal and mechanical properties, and feasibility of producing PP/MWCNT nanocomposite fiber mats by melt blowing, which has not been reported in the literature so far. Our findings implied that the melt blowing resin viscosity and the cooling of the fibers are the most critical factors in generating continuous, defect-free fine fibers. We found that MWCNT doping improved thermal stability and shifted the peak crystallization temperature to a higher temperature, indicating that MWCNTs act as nucleating agents for the PP fibers. Increasing MWCNT content significantly increased the nanocomposite's viscosity. The fiber diameter and pore size increased by 2.1-fold and 2.5-fold, respectively, while the fiber surface density decreased by 4.2-fold. Our results showed that the MWCNT doping almost doubled the MB fiber mat's specific strength. However, the fiber mat's mechanical properties deteriorated over the MWCNT content of 0.25 wt%.

We generated single-PP composites interleaved with PP/MWCNT (0.1 wt% MWCNT) MB fibers and systematically compared them with non-interleaved and pristine MB fiber mat-interleaved ones. We found that the PP/MWCNT and the pristine fiber mat-interleaved SPC's tensile modulus enhanced by 31% and 37%, respectively. Pristine fiber mat-interleaved SPC showed slightly lower tensile strength than non-interleaved one. Notwithstanding, PP/MWCNT fiber mat-interleaved SPC retrieved this loss. DIC strain field analysis implied that PP/MWCNT fiber mat interleaving resulted in robust interfacial adhesion and higher damage tolerance under tensile load. DMA analysis showed that PP/MWCNT and pristine fiber mat-interleaved SPC's storage modulus at peak tanδ enhanced by 1.6-fold and 2.2-fold than the non-interleaved one. PP/MWCNT fiber mat-interleaved SPCs had the lowest tanδ, demonstrating improvement in the overall mechanical properties of the laminates. Incorporating a low amount of MWCNTs into fiber mats and integrating them into composite structure does not add up a considerable amount to the processing and the material cost. Moreover, MB PP/MWCNT fiber mat interleaving significantly improves the interfacial adhesion and the laminae stiffness with fair recycling opportunities. In the future studies, incorporating MWCNT-doped thermoplastic veils may be used to improve the electrical conductivity of the completely insulating thermoplastic composites, for example, PP, PE, etc., for related applications.

CONFLICT OF INTEREST
The authors declare that they have no conflict of interest.

DATA AVAILABILITY STATEMENT
Data available on request from the authors.

ORCID
Yahya Kara https://orcid.org/0000-0001-6939-4114
Kolos Molnár https://orcid.org/0000-0002-9331-4652

REFERENCES

[1] S. Benlikaya, P. Riha, O. Cvelbar, *Express Polym. Lett.* **2022**, *16*, 85.

[2] N. Bagotia, D. K. Sharma, *Polym. Compos.* **1813**, *2020*, 41.

[3] I. Yasaroglu, O. Aras, Y. Kaya, *Polym. Compos.* **2022**, *43*, 1462.

[4] V. Acar, S. Erden, M. Sarıkanat, Y. Seki, H. Akbulut, M. Seydibeyoğlu, *Express Polym. Lett.* **2020**, *14*, 14.

[5] A. Pawlak, I. Vozniak, J. Krajenta, V. Beloshenko, A. Galeski, *Express Polym. Lett.* **2021**, *15*, 940.

[6] J. Lee, J. U. Lee, K. J. Lee, *Appl. Chem. Eng.* **2021**, *32*, 157.

[7] Á. D. Virág, Y. Kara, L. M. Vas, K. Molnár, *Fibers Polym.* **2021**, *22*, 2700.

[8] Y. Kara, K. Molnár, *J. Ind. Text.* **2021**, https://doi.org/10.1177/15280837211019488.

[9] J. Shi, Y. Zou, J.-X. Wang, X.-F. Zeng, G.-W. Chu, B.-C. Sun, D. Wang, J.-F. Chen, *Ind. Eng. Chem. Res.* **1962**, *2021*, 60.

[10] C. A. Stackhouse, S. Yan, L. Wang, K. Kisslinger, R. Tappero, A. R. Head, K. R. Tallman, E. S. Takeuchi, D. C. Bock, K. J. Takeuchi, *ACS Appl. Mater. Interfaces* **2021**, *13*, 47996.

[11] Y. Kara, K. Molnár, *Polym. Adv. Technol.* **2021**, *32*, 2416.

[12] B. Yu, J. Han, H. Sun, F. Zhu, Q. Zhang, J. Kong, *Polym. Compos.* **2015**, *36*, 264.

[13] M. V. Cakir, D. Kinay, *Polym. Compos.* **2021**, *42*, 5880.

[14] J. Liu, P. Yu, *Polym. Compos.* **2022**, *43*, 2450.

[15] R. R. Hegde, G. S. Bhat, *J. Appl. Polym. Sci.* **2010**, *115*, 1062.

[16] L. Cao, D. Su, Z. Su, X. Chen, *Ind. Eng. Chem. Res.* **2014**, *53*, 2308.

[17] K. Dydek, P. Latko-Durałek, A. Boczkowska, M. Sałaciński, R. Kozera, *Compos. Sci. Technol.* **2019**, *173*, 110.

[18] B. Lan, Y. Liu, S. Mo, M. He, L. Zhai, L. Fan, *Materials* **2021**, *14*, 2695.

[19] Y. Zhao, X. Ma, T. Xu, D. R. Salem, H. Fong, *Compos. Commun.* **2019**, *12*, 91.

[20] "Plastics — Determination of tensile properties — Part 4: Test conditions for isotropic and orthotropic fibre-reinforced plastic composites - ISO 527-4:2021".

[21] F.-J. Wortmann, K. Schulz, *Polymer* **1995**, *36*, 315.

[22] M. Faghihi, A. Shojaei, R. Bagheri, *Compos., B* **2015**, *78*, 50.

[23] G. R. Kasaliwal, A. Göldel, P. Pötschke, G. Heinrich, *Polymer* **2011**, *52*, 1027.

[24] I. Petrova, R. Kotsilkova, E. Ivanov, P. Kuzhir, D. Bychanok, K. Kouravelou, T. Karachalios, A. Soto Beobide, G. Voyiatzis, D. Codegoni, *Polym. Eng. Sci.* **2016**, *56*, 269.

[25] W. Xiao, S. Yu, X. Cao, K. Su, Q. Qu, Y. Tan, F. Zhao, S. Zhao, G. Zhang, A. Gao, J. Cui, Y. Yan, *Polym. Compos.* **2022**, *43*, 3858.

[26] P. Pötschke, F. Mothes, B. Krause, B. Voit, *Polymer* **2019**, *11*, 189.

[27] M. Mičušík, M. Omastová, I. Krupa, J. Prokeš, P. Pissis, E. Logakis, C. Pandis, P. Pötschke, J. Pionteck, *J. Appl. Polym. Sci.* **2009**, *113*, 2536.

[28] P.-H. Wang, S. Sarkar, P. Gulgunje, N. Verghese, S. Kumar, *Polymer* **2018**, *150*, 10.

[29] Y. T. Shieh, G. L. Liu, *J. Polym. Sci., B: Polym. Phys.* **1870**, *2007*, 45.

[30] J. Wang, Y. Kazemi, S. Wang, M. Hamidinejad, M. B. Mahmud, P. Pötschke, C. B. Park, *Compos., B* **2020**, *183*, 107663.

[31] A. Pawlak, A. Galeski, Crystallization of Polypropylene. in *Polypropylene Handbook: Morphology, Blends and Composites* (Eds: J. Karger-Kocsis, T. Bárány), Springer International Publishing, Switzerland **2019**, p. 185.

[32] S. Xin, X. Wang, *Polym. Eng. Sci.* **2012**, *52*, 1325.

[33] J. Drabek, M. Zatloukal, M. Martyn, *Polymer* **2018**, *144*, 179.

[34] R. Nayak, R. Padhye, L. Arnold, I. L. Kyratzis, Y. B. Truong, G. Peeters, L. Nichols, M. O'Shea, *Appl. Mech. Mater.* **2012**, *217-219*, 207.

[35] J. J. Henry, J. Goldbach, S. Stabler, S. Devisme, J. Chauveau, *Filtration + Separation* **2016**, *53*, 36.

[36] C. Tsioptsias, K. Leontiadis, E. Tzimpilis, I. Tsivintzelis, *J. Plast. Film Sheet.* **2021**, *37*, 283.

[37] M. V. Jose, D. Dean, J. Tyner, G. Price, E. Nyairo, *J. Appl. Polym. Sci.* **2007**, *103*, 3844.

[38] J. Zhao, G. Wang, C. Wang, C. B. Park, *Compos. Sci. Technol.* **2020**, *191*, 108084.

[39] S. H. Yetgin, *J. Mater. Res. Technol.* **2019**, *8*, 4725.

[40] K. Yu, Y. Liu, J. Leng, *RSC Adv.* **2014**, *4*, 2961.

[41] E. M. Moore, D. L. Ortiz, V. T. Marla, R. L. Shambaugh, B. P. Grady, *J. Appl. Polym. Sci.* **2004**, *93*, 2926.

[42] W. Leelapornpisit, M.-T. Ton-That, F. Perrin-Sarazin, K. C. Cole, J. Denault, B. Simard, *J. Polym. Sci., B: Polym. Phys.* **2005**, *43*, 2445.

[43] E. Ivanov, R. Kotsilkova, Reinforcement Effects of Carbon Nanotubes in Polypropylene: Rheology, Structure, Thermal Stability, and Nano-, Micro-, and Macromechanical Properties. in *Handbook of Nanoceramic and Nanocomposite Coatings and Materials* (Eds: A. S. H. Makhlouf, D. Scharnweber), Butterworth-Heinemann, United Kingdom **2015**, p. 357.

[44] S. Sonawane, P. Thakur, R. Paul, *Mater. Today: Proc* **2020**, *27*, 550.

[45] K. Lozano, E. Barrera, *J. Appl. Polym. Sci.* **2001**, *79*, 125.

[46] Y. Kara, K. Molnár, *J. Reinf. Plast. Compos.* **2022**, https://doi.org/10.1177/07316844221087736.

[47] O. Çoban, M. Özgür Bora, T. Kutluk, S. Fidan, T. Sinmazçelik, *Polym. Compos.* **2018**, *39*, 1612.

SUPPORTING INFORMATION

Additional supporting information can be found online in the Supporting Information section at the end of this article.

How to cite this article: Y. Kara, K. Molnár, *Polym. Compos.* **2022**, 1. https://doi.org/10.1002/pc.26812